Regional atmospheric patterns and the delayed sea-ice freeze-up in the western Arctic

Thomas J. Ballinger & Scott C. Sheridan

Climatic Change
An Interdisciplinary, International Journal Devoted to the Description, Causes and Implications of Climatic Change

ISSN 0165-0009
Volume 131
Number 2

Climatic Change (2015) 131:229-243
DOI 10.1007/s10584-015-1383-5

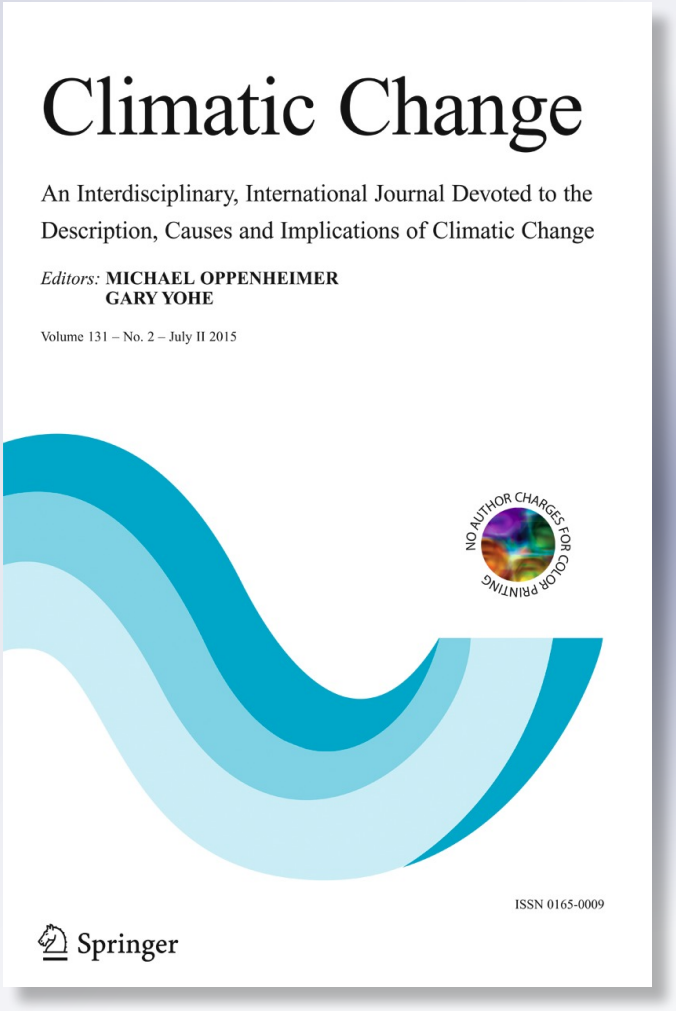

Springer

Climatic Change (2015) 131:229–243
DOI 10.1007/s10584-015-1383-5

Regional atmospheric patterns and the delayed sea-ice freeze-up in the western Arctic

Thomas J. Ballinger · Scott C. Sheridan

Received: 5 November 2014 / Accepted: 2 March 2015 / Published online: 19 March 2015

Abstract The western Arctic sea ice cover has dramatically changed since the late 1970s, particularly the timing of the autumn freeze-up. While atmospheric dynamic and thermodynamic processes associated with synoptic-scale weather patterns largely impact the onset of regional ice formation, linkages between the subseasonal occurrences of these patterns, across interannual to multidecadal time scales, and the freeze-up are not well understood. This manuscript takes a synoptic climatological atmospheric pattern (AP) classification approach to evaluate the role of warm season-dominant (i.e., May-October) mean sea-level pressure (MSLP) and 1000–500 hPa thickness APs, derived from daily NCEP/NCAR reanalysis fields, on the passive microwave-derived freeze-up dates for the marginal Beaufort/Chukchi Seas and western Arctic Ocean from 1979 to 2013. Analysis of the respective classifications' frequencies and their relationships to the freeze-up reveals that approximately one-third of freeze-up variance may be explained by early/middle warm season Beaufort Sea High surface pressure pattern frequency changes. A similar amount of freeze-up variance is explained by the occurrence of mid-warm season dominant thermal patterns, either earlier or later than their predominant season. Both results suggest that pattern changes may be associated with changing ocean–atmosphere heat exchanges affiliated with lengthened periods of melt conditions.

1 Introduction

Satellite observations since the late 1970s have confirmed substantial changes to the Arctic sea-ice cover, including extent declines during all months, highlighted by strong, negative trends during the September minimum (e.g., Simmonds 2015), decreases in thickness and volume (e.g., Stroeve et al. 2014a), and earlier melt and later freeze-up yielding expansion of the melt season (e.g., Stroeve et al. 2014b). While trend analyses on the pan-Arctic scale broadly summarize the rate of change of the ice edge, the regional (i.e., the marginal Arctic seas) ice cover behaviors throughout the annual cycle are not uniform. For instance, Comiso (2012) noted the largest multiyear ice concentration declines are found in the western Arctic

Electronic supplementary material The online version of this article (doi:10.1007/s10584-015-1383-5) contains supplementary material, which is available to authorized users.

T. J. Ballinger (✉) · S. C. Sheridan
Department of Geography, Kent State University, 413 McGilvrey Hall, Kent, OH 44242, USA
e-mail: tballin1@kent.edu

Ocean, namely the Beaufort and Chukchi Seas, which is where Xia et al. (2014) also reported the largest ice extent retreat from August to October relative to all other marginal Arctic seas.

There has been an abundance of research tracking summertime western Arctic ice edge variability and the concomitant causal mechanisms (e.g., Rogers 1978; Drobot and Maslanik 2003; Ballinger and Rogers 2013). However, much less research has been conducted regarding the factors connected to Arctic sea ice melt season changes, especially as it relates to the temporal patterns of the autumn ice cover freeze-up. Stroeve et al. (2014b) found statistically significant negative trends in melt onset dates in the Beaufort (−2.3 days decade^{-1}) and Chukchi (−2.7 days decade^{-1}) Seas from 1979 to 2013, with resulting changes in albedo due to ice melt extending the period of significant solar heating of the region's open ocean. Increased heat input into the ocean during the warm-season delays the freeze-up (Vihma 2014), and partially explains the observed sea surface temperature (SST) and surface air temperature (SAT) increases in the western Arctic region, which act to slow the rate of sea-ice formation as the open ocean gradually cools with diminishing insolation through autumn (e.g., Wood et al. 2013; Stroeve et al. 2014b). Changes in ocean-to-atmosphere heating due to later ice cover formation have been recognized as a substantial culprit for recent autumn lower-tropospheric warming (e.g., Overland 2009; Serreze et al. 2009) and may be connected to the amplified (blocking) nature of large-scale atmospheric flow and persistence of synoptic scale weather systems in the Northern Hemisphere high and middle latitudes in recent years due to a reduction in the high/middle latitude temperature gradient (e.g., Francis and Vavrus 2012; Tang et al. 2014).

There are ultimately several dynamic and thermodynamic mechanisms that can explain some of the interannual to multidecadal variability of the western Arctic sea ice pack throughout different portions of the annual cycle. Wu et al. (2014) noted increasing trends in MSLP magnitudes and associated strengthening summer and autumn anticyclonic surface winds over the western Arctic from 1979 to 2012. Ogi and Wallace (2012) and Overland et al. (2012) linked early summer 925-hPa anticyclonic wind field anomalies and positive 700-hPa geopotential height anomalies, respectively, over the western Arctic to abrupt summertime Arctic sea-ice losses since 2007. Candlish et al. (2014) explored relationships between wind speed/direction and SAT to western Canadian Arctic sea-ice concentration and found a statistically significant, negative ($r=-0.88$, $p<0.05$) 1-month lagged correlation between summer/autumn SATs and Beaufort sea ice from 1981 to 2010, indicating that a rise in air temperature forces the subsequent month's decline in sea ice. However, wind speed and direction were secondary predictors of ice concentration variability in their analyses.

While deviations and anomalies from mean seasonal atmospheric circulation fields are more commonly used, synoptic climatological methods, particularly atmospheric pattern (AP) classification, have been effectively utilized to holistically understand the spectrum of common, daily weather patterns and their temporal variability related to regional cryospheric change in the high northern latitudes (e.g., Mote 1998; Maslanik et al. 2007; Fettweis et al. 2011, 2013; Bezeau et al. 2014). Most of the western Arctic-centric synoptic-typing schemes have been dynamical in nature, relating the region's ice cover variables to the seasonal and subseasonal occurrence of mean sea-level pressure (MSLP) patterns. Asplin et al. (2009) associated seasonal mean MSLP AP frequency composites, constructed via k-means cluster analysis, to examine sea-ice motion in the Beaufort Sea from 1979 to 2006. Ballinger and Sheridan (2014) used a two-step cluster (TSC) analysis technique to generate a MSLP AP catalogue and statistically relate the monthly occurrence of melt season-dominant patterns against September sea-ice extent variability across the western Arctic Ocean from 1979 to 2011.

While variables such as ice extent and motion have been studied with respect to atmospheric pattern variability, little research has evaluated links between sea ice freeze-up and atmospheric changes. Better understanding of atmospheric conditions influencing the freeze-up onset is critical to improved modeling of high-latitude ocean–atmosphere heat exchanges and assessment of cryospheric impacts on high/middle latitude weather conditions. To explore these connections, this research takes a synoptic-typing approach to better understand the temporal role that dynamic (i.e., MSLP) and thermodynamic (i.e., 1000–500 hPa thickness) atmospheric patterns are having on changes observed of the western Arctic sea ice freeze-up from 1979 to 2013. These relationships are analyzed over different time periods to evaluate how the interannual and multidecadal monthly temporal variability of the pressure and thickness patterns' relate to the onset of the continuous sea ice formation. This manuscript is subdivided as follows; Section 2 discusses the sea ice and reanalysis datasets used in the study. Section 3 outlines the synoptic climatological methods employed to construct the respective atmospheric pattern classifications. Section 4 describes the results, which include a monthly climatology of the classified patterns, temporal composites that highlight the respective patterns' frequency changes relative to the timing of sea ice formation, and statistical associations between the patterns' occurrences and the freeze-up dates. Section 5 discusses the results, while Section 6 provides brief, concluding remarks on the analyses, and suggests future directions for integrated western Arctic climate and sea ice freeze-up research.

2 Data

2.1 Reanalysis fields

Daily-averaged, raw fields of mean sea-level pressure (MSLP) and geopotential-height data used to calculate the 1000–500 hPa thicknesses are obtained from the National Centers for Environmental Prediction/National Center for Atmospheric Research (NCEP/NCAR) first generation reanalysis (Kalnay et al. 1996) for all calendar days over the 1979–2013 period (n=35 years). The gridded data are analyzed at a 2.5° latitude/longitude horizontal resolution and two domains are utilized; MSLP fields are mapped from 50–90°N and 150°E-100°W (721 gridpoints), while the 1000–500 hPa thickness data are displayed in a smaller domain across 70–85°N and 150°E-100°W (315 gridpoints). Justification for the use of these disparate domains is provided in the Methodology section. NCEP/NCAR MSLP and geopotential-height fields are selected because these model-derived fields closely follow available observational data (Kalnay et al. 1996) and these respective fields yield similar atmospheric flow patterns as other reanalysis products as corroborated by recent western Arctic research (e.g., Serreze and Barrett 2011; Moore 2012). Further, the respective datasets may be used to infer numerous atmospheric conditions, including near-surface wind speed and direction and cloud cover (MSLP), and thermal conditions and associated atmospheric flow of the middle/lower portion of troposphere (1000–500 hPa thickness), respectively.

2.2 Sea ice data

The western Arctic sea ice freeze-up, referencing the date of continuous freeze conditions observed in a particular pixel, is calculated from passive microwave satellite-derived data for the 1979–2013 period. The satellites employed in constructing the freeze-up record include the Nimbus 7 Scanning Multichannel Microwave Radiometer, and the Defense Meteorological Satellite Program "F family" satellite platforms hosting the Special Sensor Microwave/Imager

and the Special Sensor Microwave Imager/Sounder. The algorithm used to process the data is summarized in both Markus et al. (2009) and Stroeve et al. (2014b). Data are obtained at a 25× 25 km horizontal resolution across the Chukchi (66.5–77.3°N, 177°E-156.5°W) and Beaufort Seas (71.2–77.3°N, 156.5°W-125°W) in the western Arctic Ocean. The data is quality checked and pixels not registering a date are removed. All pixels that record a freeze-up date are then averaged across the domain of each marginal Arctic sea to construct the annual mean freeze-up date for each year in the study period. The annual mean western Arctic freeze-up date is also constructed and represents the average of all pixel-registered freeze-up dates in the Beaufort and Chukchi Seas for a particular year. Since the Pearson bivariate correlation coefficient between the freeze-up datasets for these marginal seas reveals slight divergence in interannual variability ($r=+0.77$, $p<0.01$), particularly during the mid-2000s (Figure S1), associations between the synoptic types and the Beaufort, Chukchi, and areal western Arctic ice cover are all separately explored.

While sea ice freeze-up represents the primary environmental variable of interest in this synoptic climatological study, a time series of melt onset dates (i.e., marking the beginning of continuous melt) is also created from the aforementioned data sources and methods (Figure S2). The difference between the respective onset of continuous melt and freeze-up conditions represents the temporal boundaries of the melt season (synonymous with "warm season" throughout this manuscript) and are used to constrain the forthcoming analysis described in Section 4.

3 Methodology

3.1 General overview of the TSC analysis

Synoptic climatological classification often involves an atmospheric pattern (AP) methodological approach, which describes the range of typical synoptic scale weather patterns observed at a particular atmospheric level (Yarnal 1993). This study employs the AP approach to relate MSLP and 1000–500 hPa thickness synoptic types to the freeze-up of the western Arctic Ocean. Since it is desired to analyze the magnitude and seasonality of all patterns with respect to the aforementioned freeze-up, no adjustments were made to the raw reanalysis data prior to initiating the classifications. The synoptic AP classifications, conducted using SPSS Statistics Version 19.0, are initiated by subjecting all gridpoints in each domain to an unrotated S-mode correlation matrix-based principal component analysis (PCA), which reduces the influence of spatial autocorrelation amongst neighboring gridded values and simplifies the dataset while maintaining the bulk of its original explained variance. The retained principal components (PCs) are then entered into a two-step cluster (TSC) analysis in which the first step classifies the initial day's synoptic field (1 January 1979) as the first AP, while the second step initiates a hierarchical clustering procedure that either classifies the second day with the original AP or creates a new AP. This process continues until all days in the dataset are classified into a stipulated number of APs of similar magnitude and spatial orientation that are distinct from other patterns created. More descriptive details of the TSC analysis for synoptic climatological research may be found in Coleman and Rogers (2007).

3.2 Construction of the MSLP AP classification

Statistical techniques employed by Ballinger and Sheridan (2014; abbreviated B&S hereafter in this section) revealed robust correlations between monthly MSLP pattern frequencies and

the western Arctic summer sea-ice extent minima, 1979–2011. For use in this research, the addition of 2012 and 2013 MSLP data is necessary. This integration is carried out using a multi-step procedure similar to that outlined in Lee and Sheridan (2012). The B&S classification details are briefly summarized first. PCA was conducted on all MSLP gridpoints and generated 26 PCs with eigenvalues of at least 1.0, accounting for 98.15 % of the original dataset variance. Those retained PCs were then subjected to TSC analysis (with the log-likelihood distance measure selected) and 15 APs were generated.

A stepwise multiple linear regression model is then used to merge the 2012–2013 data, where all 26 PCs from the B&S classification are separately regressed onto each of the 721 gridpoints of the complete 1979–2013 MSLP time series. The unstandardized predicted values (i.e., virtual PCs) derived from the regression analysis are saved in order to maintain the spatial properties of the 15 APs previously created. Discriminant function analysis (DFA) is then employed; the 15 APs from the B&S classification are collectively defined as the grouping variable while the virtual PCs represent the independent values for training the new classification with the 2012 and 2013 MSLP data. After these procedures are executed, a new, consistent classification comprised of 15 mean sea-level pressure patterns (abbreviated P1, P2,…P15 in forthcoming sections) is generated that is spatiotemporally similar to B&S in terms of the appearance of the patterns and their co-occurrence (82.94 %) during overlapping time periods (i.e., 1979–2011).

3.3 Creation of the 1000–500 hPa thickness classification

Initially, a 1000–500 hPa thickness classification was created using the same domain as the MSLP classification described previously. However, preliminary analysis revealed no statistically significant ($p \leq 0.05$) Pearson bivariate correlations between May-October monthly AP frequencies (i.e., during the western Arctic melt season) and the western Arctic freeze-up dates. Therefore, several subdomains within the MSLP domain were created and similar monthly frequencies were correlated with the freeze-up data before the final domain was selected. Ultimately, the 70–85°N, 150°E-100°W domain is chosen for forthcoming analyses because this domain yields the largest number of statistically significant AP correlations with the freeze-up date time series.

The 1000–500 hPa thickness classification is produced in a manner similar to the MSLP classification. An unrotated, correlation matrix-based PCA is conducted on all gridpoints in the analysis and yields 7 PCs with eigenvalues of at least 1.0, explaining 98.89 % of the original dataset variance. Those 7 PCs are subjected to TSC analysis (with the log-likelihood distance measure designated) and 15 thickness patterns (abbreviated T1, T2,…T15 in forthcoming sections) are generated.

4 Results

4.1 Frequency analysis

4.1.1 MSLP classification

The monthly mean frequencies of 15 sea-level pressure patterns are presented in Table S1, while all synoptic pattern maps are displayed in Figure S3. Pattern frequencies are roughly distributed throughout the year and aside from P9 during January (i.e., P9 January) and P1

November, which both occur 17 % of days in those months, no other pressure patterns occur at least 13 % days month^{-1} outside of warm-season months May-September. During these months, P11-14 (Fig. 1) occur much more frequently relative to the other 11 patterns during these months or over the remaining months of the year (i.e., November-April). P11 occurs 37 % (33 %) of all June (July) days. P12 and P13 have similar seasonality, occurring most often during August (35 % and 31 % of days respectively), followed by slightly lesser frequencies in July and June. P14 is early warm season-dominant and occurs most often during May (21 % of days).

All remaining analyses are constrained to the warm season-dominant P11-14 for several reasons. The mean absolute correlation coefficients of the western Arctic freeze-up dates and all AP frequencies aggregated by month reveal a general peak during May-October (see Table S2). This window of months typically frames the western Arctic melt season (i.e., sea ice melt onset until freeze-up) as melt onset dates have commenced from late May (e.g., Day of Year=148; Figure S2), while freeze-up has often transpired during October (e.g., Day of Year$_{1979\text{-}2013\mu}\approx$277; Figure S1). Further, of the 8 statistically significant correlation coefficients between May-October MSLP pattern frequencies and the western Arctic freeze-up record, 5 involve P11-14 (Fig. 1; more statistical details are offered in Section 4.3).

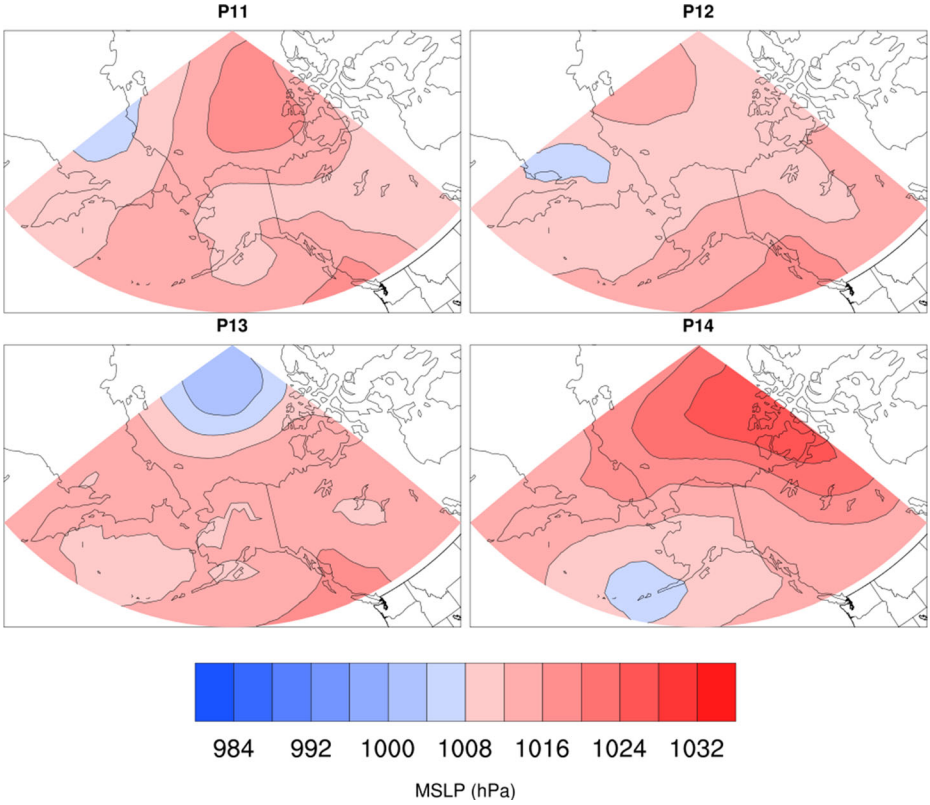

Fig. 1 Warm season-dominant MSLP patterns P11-14. See Figure S3 for the full catalogue

4.1.2 1000–500 hPa thickness classification

Monthly mean frequencies of the thickness patterns are displayed in Table S3 and the complete thickness pattern classification is shown in Figure S4. These 15 patterns display a more distinctive seasonality, compared to the MSLP patterns, with several patterns predominantly occurring during the cold (i.e., November-April) *or* warm seasons. For instance T1 January and February occur 17 % and 19 % of all days in those respective months, while the pattern's occurrence during June-September is negligible. However, no cold season-dominant patterns occur more than 19 % of days month^{-1}. With the exception of T6, whose maximum frequency of occurrence is 15 % of July days, all other warm season-dominant patterns (T6, T9, and T13-15; Fig. 2) occur on at least 1 month during 22 % of days or more.

Similar to the MSLP analyses, remaining 1000–500 hPa thickness pattern analyses focus on warm season-dominant T6, T9, and T13-15. In particular, mean absolute correlation coefficients among the monthly thickness pattern frequencies and western Arctic freeze-up dates are typically highest during May-October (Table S2), matching the western Arctic melt season temporal domain. Statistically significant AP correlations with the western Arctic sea ice freeze-up dates also largely transpire during these months, with 6 of the 11 total significant correlations observed with T6, T9, T13 and T15 (more statistical details may also be found in Section 4.3).

4.2 Assessing AP temporal differences through compositing

4.2.1 MSLP

As seen in Figure S1, western Arctic freeze-up has been dramatically delayed since the late 1990s relative to the previous years dating back to 1979. Warm-season dominant pressure patterns P11-14 are sequentially composited in seven equal quintiles (i.e., Early, 1979–1985; Early-Middle, 1986–1992; Middle, 1993–1999; Middle-Late, 2000–2006; Late, 2007–2013)

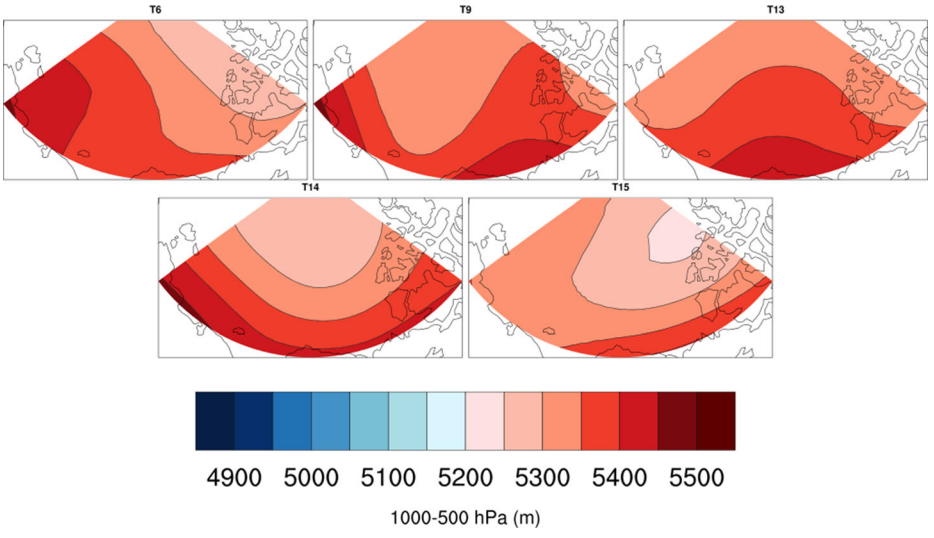

Fig. 2 Warm season-dominant 1000–500 hPa thickness patterns T6, T9, and T13-15. See Figure S4 for the full catalogue

to evaluate if their monthly occurrences in successive periods throughout the time series may be associated with changes in the date of the freeze-up (Fig. 3). Interquintile comparisons reveal substantial changes between periods, particularly more recently. P11, which resolves a Beaufort Sea High (BSH) pattern, has exhibited a notable increase in frequency during the Late versus Middle-Late periods for June (+4.14 days year^{-1}) and July (+4.43 days year^{-1}), while P11 August frequencies also occur much more frequently during the later freeze-up years since 2000 relative to the previous three periods. To assess intramonthly changes across the warm season, the cumulative frequency of P11 classified days (May-October) within each quintile, for instance, is calculated and a 14-day centered moving average is applied to smooth the time series and assess the frequency variability between the Early, Middle, and Late periods (Figure S5). During June, July, and August (JJA) P11 occurs much more frequently during the last 7 years of the study period relative to those same months during the Middle and Early portions of the record, which may be associated with the substantial summertime retreat of the region's ice edge (Ballinger and Sheridan 2014) and may potentially contribute to the recent persistence shown in the freeze-up record.

As shown in Fig. 3, the increase in the number of P11 classified days during the core of the warm season (JJA) is offset by the sharp decrease of P12 during June and July and more subtle declines of P13 for those same months during the Late period. P13 August frequencies also drop considerably from the Middle to Late periods (−4.57 days year^{-1}), which compensate for P11 frequency increases during this month.

P14, a broader, stronger high pressure pattern compared to P11, has also occurred much more often during May from the Middle-Late to Late quintiles (+3.71 days year^{-1}), and then occurs infrequently from June-October relative to the other three main MSLP patterns (see Fig. 3). This particular pressure pattern may represent a more spatially-extensive BSH pattern

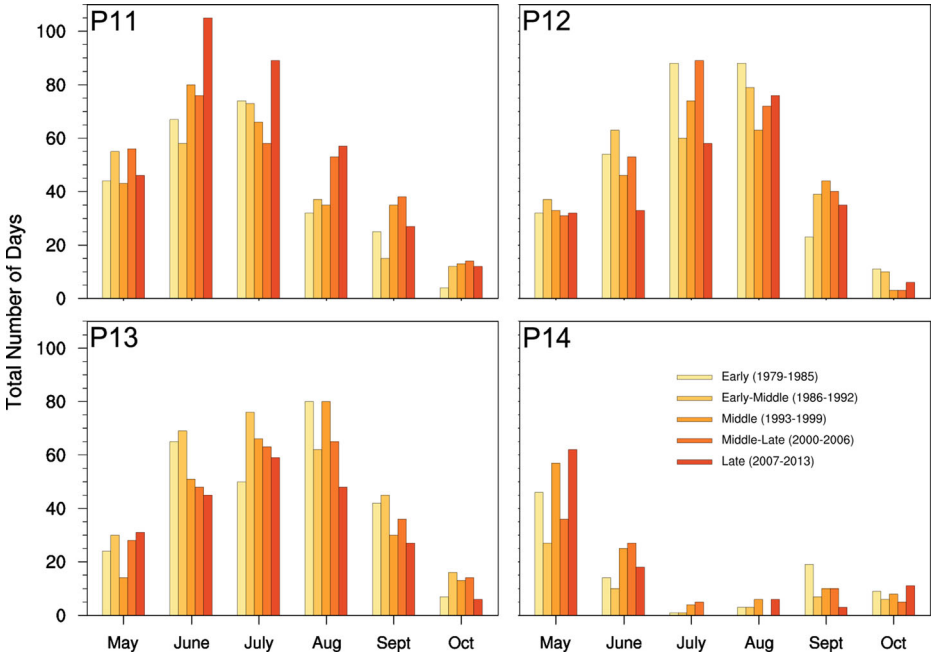

Fig. 3 Quintiles of P11-14 frequencies by warm season months, May – October. Each quintile represents a consecutive 7-year period across the entire time series (1979–2013)

and relate to the mid-tropospheric anticyclonic circulation that has been observed (with increasing frequency) stretching across the western Arctic to Greenland over a similar time period (Bezeau et al. 2014).

4.2.2 1000–500 hPa thickness

The thickness pattern frequencies are aggregated similarly to the pressure patterns discussed previously, and substantial frequency differences observed amongst the different periods are discussed here (and seen in Fig. 4). During the Early, Early-Middle, and Middle-Late periods T6 May occurs relatively infrequently compared to the Middle and Late Periods and these frequency spikes are roughly coincident with periods of later freeze-up. T9 also exhibits an increase from Middle and Middle-Late to Late periods during May (+1.14 days year^{-1}) and September (+1.57 days year^{-1}). These frequency increases from the Early and Middle periods to the Late period are largely manifested in the latter halves of those respective months (Figure S6).

Increased occurrence of the T13 thermal ridge over the western Arctic Ocean from the Middle-Late to Late periods for June (+2.43 days year^{-1}), July (+2.57 days year^{-1}), and August (+3.43 days year^{-1}) may collectively explain some of the persistence of the freeze dates over these periods (e.g., Middle-Late Day of Year (DOY) Freeze-up$_{\mu}$=279 versus Late DOY Freeze-up$_{\mu}$=295). The T13 increases are balanced by declines of T14 during the aforementioned months (Fig. 4). The late warm-season increases of T15 September and October from the Middle-Late to Late periods, represented by a strong thickness gradient over the eastern half of the domain, may also offer physical explanation for the recent expansion of the western Arctic freeze-up period.

4.3 Statistical analyses

4.3.1 MSLP

The multiyear/short-term (i.e., 7-year) frequency changes of atmospheric patterns assessed in Section 4.2 are likely playing a role in freeze-up change as the ice edge continues to retreat

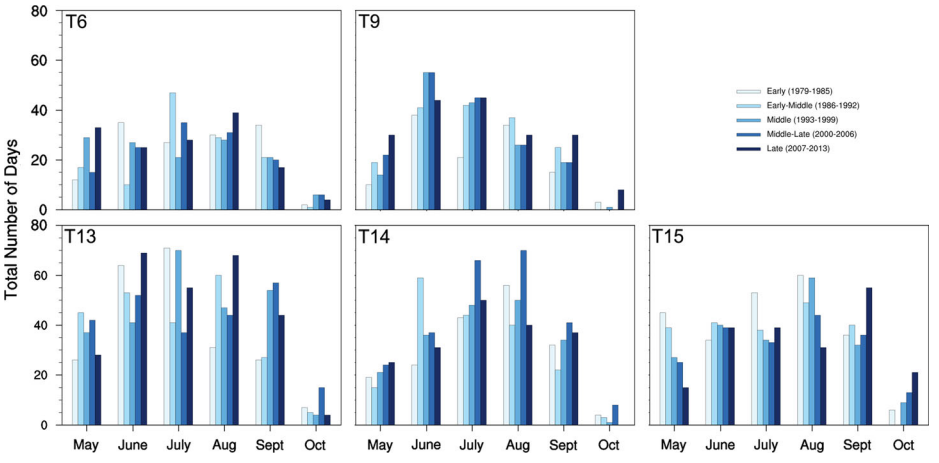

Fig. 4 Quintiles of T6, T9, and T13-15 frequencies by warm season months, May – October. Each quintile represents a consecutive 7-year period across the entire time series (1979–2013)

poleward through summer, but the low-frequency (i.e., multidecadal) behaviors of the APs are also likely fueling freeze date persistence over time. To test this notion, Pearson bivariate correlations and stepwise multiple linear regression analyses involving the frequencies of the warm season MSLP patterns and Beaufort, Chukchi, and western Arctic freeze-up time series are performed in order to statistically evaluate individual and collective pressure pattern associations with the variability of the annual freeze dates.

As shown in Table S4, there are several patterns whose monthly frequencies are statistically connected to the timing of the freeze-up in the Beaufort, Chukchi, and western Arctic and these significant associations often occur in May, June, August, and September. Increases in P14 May, reflected by prevalence of high pressure stretching across most of the northernmost portion of the region, yields a tendency for delayed freeze-up across all three ice domains. Moreover, P11 June is positively correlated with freeze dates of the Beaufort ($r=+0.34$, $p=0.044$), Chukchi ($r=+0.42$, $p=0.012$), and western Arctic ($r=+0.42$, $p=0.013$) domains. P11 August frequencies also exhibit similar multidecadal covariability with the Chukchi Sea ($r=+0.40$, $p=0.018$) and western Arctic ($r=+0.36$, $p=0.036$), suggesting that early and middle warm season increases of BSH patterns also facilitate later freeze dates.

The monthly pressure patterns significantly correlated with the respective ice data, displayed in Table S4, are used as predictors against those freeze-up time series in three separate stepwise multiple linear regression models. The freeze-up explained variance (i.e., adjusted r^2) by the significant frequencies is similar across the western Arctic Ocean and Beaufort and Chukchi Seas. P11 June and P13 August account for 30 % (31 %) of the cumulative freeze-up variance across the western Arctic (Chukchi Sea) and offer some statistical explanation between early/middle warm season-dominant regional high pressure patterns' variability and delayed ice formation in the referenced domains. MSLP pattern predictors for the Beaufort Sea freeze-up include P12 June and P14 May (cumulative $r^2=28$ %), and excludes the P11 BSH pattern that explains some freeze-date variance of the larger sea-ice domains.

4.3.2 1000–500 hPa thickness

The significant correlations between the thickness pattern frequencies and the sea ice freeze-up share similar subseasonal associations with the MSLP results described in the previous section, and there is a clear seasonal signal derived from early and middle/late warm season thickness pattern occurrences (Table S4). May occurrences of T6 and T9 are positively correlated with freeze-up across most of the domains, indicating that the increase of these patterns during the early season from 2007 to 2013 potentially prompt later freezes through earlier melting of the ice pack.

T13 exhibits a warm ridge over the Beaufort Sea and its August and September frequencies are positively correlated with the sea ice in the Chukchi and greater western Arctic Ocean. In particular, T13 August frequencies (Fig. 4) dramatically increase with freeze-date persistence during recent years, while T13 September frequencies have generally been much higher since the Middle period (i.e., 1993–1999). T15 August, and its associated weak thickness gradient across the domain, shows a negative linear relationship with the ice freeze-up in the Chukchi Sea and western Arctic Ocean, likely since its decline has been associated with the noted T13 frequency increase. In contrast, when T15 occurs more frequently during October, as has been observed over the Late period, freeze dates tend to be later. The correlation coefficient between this pattern's monthly frequency and the freeze-up is highest in the Chukchi Sea ($r=+0.52$, $p=0.002$) and western Arctic ($r=+0.47$, $p=0.004$) relative to all thickness patterns explored via correlation analysis.

Stepwise multiple linear regression modeling using the significant, monthly thickness patterns linked to the freeze-up dates as predictors reveals similar variance contributions for the ice domains as found in the MSLP regression analyses (Table S4). Nearly one-third of the western Arctic freeze-up is collectively represented by T15 October and T9 May frequencies (r^2=29 %). Similarly, T15 October is the initial predictor of Chukchi freeze-up, and combines with T13 September to explain 33 % of the variance. The Beaufort Sea ice freeze dates are only weakly explained by T9 May (r^2=12 %). While few thickness patterns explain roughly one-third or less of the respective freeze date variability since 1979, regression fits suggest the cumulative importance of early and late-warm season thermal patterns to explaining some freeze-up variability across much of the western Arctic region.

4.3.3 MSLP and 1000–500 hPa thickness contributions

The monthly frequency variability of MSLP patterns *or* 1000–500 thickness patterns discussed previously are linked to greater ice loss at certain times through the warm season than others. For instance, P11 June frequency increases coinciding with the maximization of solar insolation during that month aid the summer ice pack melt and its dynamical movement. However, the collective influence of MSLP *and* 1000–500 hPa thickness pattern occurrences during the melt season may also influence the autumn ice formation over time.

In order to evaluate this collective contribution by both disparate synoptic catalogues, all statistically significant patterns shown in Table S4 for each domain are entered into stepwise multiple linear regression models to evaluate their ability to hindcast the respective regions' freeze-up dates. The amount of collective variance explained by the predictors is consistent amongst the 3 domains (total r^2=38–41 %). P12 June, P14 May, and T14 May collectively account for 39 % of the Beaufort Sea freeze-up variability. Chukchi Sea freeze-up can be explained by three predictors (total r^2=41 %), which include T15 October, T9 May, and P13 September, while the western Arctic cover (total r^2=38 %) can also partially be explained by those same predictors.

Despite the omission of P11, particularly during June, as a statistically significant predictor in the collective regression model runs, its recent quintile frequency increases (i.e., 2007–2013, see Fig. 3) are substantial relative to earlier time periods, and the multidecadal statistical links to the freeze-up (Table S4) are relatively strong. Recent AP classifications have similarly corroborated the summertime increase of the BSH pattern (e.g., Ballinger et al. 2014; Belleflamme et al. 2015), and a statistical connection between its early warm season occurrence and the observed September Beaufort and Chukchi sea ice extent minima (Ballinger and Sheridan 2014).

5 Discussion

5.1 MSLP

BSH pressure patterns have increased across the early/middle warm season months in recent years. These substantial increases in the BSH frequencies (e.g., P11 JJA or P14 May) create a dynamic environment ideal for sea-ice movement with a synoptic setup promoting large-scale subsidence and southerly flow over the Beaufort and Chukchi Seas. Melt conditions would be particularly optimal when these pressure patterns persist during the early and middle portions of the warm season as clear skies allow diabatic heating of the sea ice surface and shortwave radiation absorption into the open ocean adjacent to the ice edge, which enhances the ice-albedo feedback.

Decreases in P12 and P13 JJA frequencies compensate for some of the observed BSH (i.e., P11) increases during those months. P12 represents a relatively weak pressure gradient across the western Arctic and it is no surprise that a decrease in its frequency coincides with a later freeze-up (negative correlation coefficient) since this pattern's general frequency decreases over time (as witnessed in Fig. 3) are paralleled by P11 increases. This sharp change in occurrence of low-pressure patterns (e.g., P13) to high pressure patterns in the western Arctic (e.g., P11 and P14) may partly explain the freeze-up delays into later autumn. Moreover, correlation coefficients between P13 August and September frequencies and all three domains' freeze-up are also negative; northerly, cold air advection fueled by the low-pressure cell located in the central Arctic Ocean would yield conditions more conducive to earlier ice-cover formation. P11 has increased during August since 2000 and offsets some observed declines in P13 frequencies during that month, which may also partially explain why freeze-up dates are transpiring later in the year over recent years.

5.2 1000–500 hPa thickness

T6 May and T9 May/September thickness pattern frequency increases in recent years are likely playing a role on sea-ice conditions. Thicknesses of ~5300–5450 m are prevalent across the domain of both patterns. Coastal areas, including northern Siberia (T6) and northern Alaska and Siberia (T9), are encompassed by the 5450-m contour, with lower thickness values stretching poleward. This particular thickness value represents a proxy for near-freezing surface air temperatures, and its prevalence over the ocean may aid changes in freeze-up either through enhanced sea-ice melting early in the warm season (i.e., during May), delayed ice formation during the latter portion of the warm season (i.e., during September), or a combination of both mechanisms. It should also be noted that the relatively meridional orientation of both thickness patterns' isopachs yields a thermal wind regime that advects warmer, southerly air off the adjacent landmasses toward the open ocean and adjacent ice pack thereby promoting the thermodynamic melting and slowing of the subsequent formation of ice cover described.

Increases in T13 August and September frequencies are statistically linked with Chukchi and western Arctic freeze dates. Near-freezing air temperatures inferred from the thermal ridge of 5450-m thickness values in the south-central portion of the domain and the associated off-continent, southwesterly flow may act to postpone sea-ice formation. The inverse association between T15 August frequencies and the freeze dates may largely be the result of recent, coincident increases in T13 (see Fig. 4) that exacerbate sea ice melt and ultimately delay freeze onset.

The relationship between T15 and freeze-up timing appears to change as the warm season progresses. Whereas decreases (increases) of T15 August are tied to later (earlier) western Arctic and Chukchi Sea freeze-ups, the correlation coefficient flips sign and strengthens during October and direct associations can be made between T15 occurrences and the aforementioned domains' freeze dates. T15 October's increase from pre-1999 to the years since 2007 is roughly by a factor of two (Fig. 4). This substantial frequency change may be driven by long-term changes to the ice cover. From 1979 to 2012, the October open water fraction (inversely related to sea-ice concentration trends) increased 44 % and 46 % in the Beaufort and Chukchi Seas, respectively; this generates increases in oceanic sensible heat release to the atmosphere and lower tropospheric warming as evidenced by strong, positive linear trends in Barrow, Alaska's surface air temperatures over the period (Wendler et al. 2014). This could manifest in T15's prolonged occurrence during October relative to previous years. Hence the ice cover changes through October, including the observed freeze-date persistence in recent

years, may be expanding the seasonality of the typical warm-season weather patterns in the western Arctic and altering thermodynamic associations with the sea ice cover over time.

6 Conclusions

This study utilizes two synoptic climatological classifications, derived from MSLP and 1000–500 hPa thickness data, to explore the observed changes in sea ice freeze-up dates in the western Arctic. Both classifications show clear changes in their respective patterns over the 7-year windows, particularly in the Late period (i.e., 2007–2013) for the patterns exhibiting statistically significant associations with the ice dates. Moreover, the frequency variability of the early/middle warm season MSLP patterns and early/late warm season thickness patterns are largely related to the timing of the seasonal sea-ice cover formation during autumn (i.e., September-November). Correlation analyses and multiple linear regression models applied to assess the cumulative impacts of both classifications' pattern frequencies on freeze-up timing suggest that the influence of thermal patterns may be more important than the wind-driven forcing, especially for those patterns occurring late in the warm season with high thickness values and associated air temperatures near the freezing point extending over the ocean.

There are undoubtedly a multitude of atmospheric mechanisms that contribute to the interannual and multidecadal degradation and thinning of the western Arctic summer ice cover (e.g., Ballinger and Rogers 2013), leading to freeze-up persistence. Factors including Northern Hemisphere temperature increases and warm season atmospheric teleconnection phases involving the Arctic Dipole, Arctic Oscillation, and Pacific-North American Pattern have also been shown to account for a significant portion of the region's summer sea-ice extent variance over the last two decades (e.g., Ballinger and Rogers 2014) and may further elucidate some of the residual regression model freeze-up variance presented in this manuscript. Substantial thinning of the ice pack during the last decade, particularly in the western Arctic (e.g., Kwok and Cunningham 2010), suggests that anomalous frequencies of atmospheric patterns may play an increasingly significant role in massive seasonal sea-ice losses and therefore these relationships should continue to be monitored, particularly as linkages between freeze-up and weather pattern changes become elucidated through continued cryospheric research.

This limited-domain synoptic typing study has been shown to be effective at capturing typical, synoptic scale patterns and their recent frequency increases (i.e., the BSH) that have also been resolved through different classification approaches, alternative reanalysis products, and larger domains (e.g., Bezeau et al. 2014; Belleflamme et al. 2015). Future work exploring various atmospheric pressure levels' geopotential height and wind field associations to the freeze-up may be helpful, for instance, at further explaining the residual variance of the linear best fit models presented in this manuscript. A spatial expansion of both the sea ice and atmospheric domains may also be useful to assess and compare the impacts of high latitude atmospheric pattern variability, and related dynamic and thermodynamic processes, to freeze-up changes observed in other marginal Arctic seas.

Acknowledgments The authors would like to thank Jeffrey Miller (NASA Cryospheric Sciences Laboratory/Wyle, Inc.), Stephen Howell (Environment Canada), Mary Haley (NCAR/CISL), and Cameron Lee (Kent State University, Department of Geography) for their assistance with aspects of data acquisition/processing and figure creation.

The NCEP/NCAR reanalysis data is obtained from the NOAA/ESRL Physical Science Division (http://www.esrl.noaa.gov/psd/data/reanalysis/ reanalysis.shtml), while the freeze-up data is acquired from the NASA

Cryosphere Science Research Portal (http://neptune.gsfc.nasa.gov/csb/index.php?section=54) with updates for 2012 and 2013 supplied by Jeffrey Miller.

References

Asplin MG, Lukovich JV, Barber DG (2009) Atmospheric forcing of the Beaufort Sea ice gyre: surface pressure climatology and sea ice motion. *Journal of Geophysical Research* 114: C00A06. doi:10.1029/2008JC005127

Ballinger TJ, Rogers JC (2013) Atmosphere and ocean impacts on recent western Arctic summer sea ice melt. Geography Compass 7:686–700. doi:10.1111/gec3.12077

Ballinger TJ, Rogers JC (2014) Climatic and atmospheric teleconnection indices and western Arctic sea ice variability. Physical Geography 35:459–477. doi:10.1080/02723646.2014/949338

Ballinger TJ, Sheridan SC (2014) Associations between circulation pattern frequencies and sea ice minima in the western Arctic. International Journal of Climatology 34:1385–1394. doi:10.1002/joc3767

Ballinger TJ, Sheridan SC, Hanna E (2014) Resolving the Beaufort Sea high using synoptic climatological methods. International Journal of Climatology 34:3312–3319. doi:10.1002/joc.3907

Belleflamme A, Fettweis X, Erpicum M (2015) Recent summer Arctic atmospheric circulation anomalies in a historical perspective. The Cryosphere 9:53–64. doi:10.5194/tc-9-53-2015

Bezeau P, Sharp M, Gascon G (2014) Variability in summer anticyclonic circulation over the Canadian Arctic Archipelago and west Greenland in the late 20th/early 21st centuries and its effect on glacier mass balance. *International Journal of Climatology*, in press. doi:1002/joc.4000.

Candlish LM, Iacozza J, Lukovich JV, Horton B, Barber DG (2014) Sea ice climatology in the Canadian Western Arctic: thermodynamic *versus* dynamic controls. *International Journal of Climatology*, in press. doi:10.1002/joc.4094.

Coleman JSM, Rogers JC (2007) A synoptic climatology of the central United States and associations with Pacific teleconnection pattern frequency. Journal of Climate 20:3485–3497. doi:10.1175/JCLI4201.1

Comiso JC (2012) Large decadal decline of the Arctic multiyear ice cover. Journal of Climate 25:1176–1193. doi:10.1175/JCLI-D-11-00113.1

Drobot SD, Maslanik JA (2003) Interannual variability in summer Beaufort Sea ice conditions: Relationship to winter and summer surface and atmospheric variability. *Journal of Geophysical Research* 108. doi:10.1029/2002JC001537

Fettweis X, Mabille G, Erpicum M, Nicolay S, Van den Broeke M (2011) The 1958–2009 Greenland ice sheet surface melt and the mid-tropospheric atmospheric circulation. Climate Dynamics 36:139–159. doi:10.1007/s00382-010-0772-8

Fettweis X, Hanna E, Lang C, Belleflamme A, Erpicum M, Gallée H (2013) Important role of the mid-tropospheric atmospheric circulation in the recent surface melt increase over the Greenland ice sheet. Cryosphere 7:241–248

Francis JA, Vavrus SJ (2012) Evidence linking Arctic amplification to extreme weather in mid-latitudes. *Geophysical Research Letters* 39: L06801. doi:10.1029/2012GL051000

Kalnay E, Kanamitsu M, Kistler R, Collins W, Deaven D, Gandin L, Iredell M, Saha S, White G, Woollen J, Zhu Y, Chelliah M, Ebisuzaki W, Higgins W, Janowiak J, Mo KC, Ropelewski C, Wang J, Leetmaa A, Reynolds R, Jenne R, Joseph D (1996) The NCEP/NCAR 40-year reanalysis project. Bulletin of the American Meteorological Society 77:437–471

Kwok R, Cunningham GF (2010) Contribution of melt in the Beaufort Sea to the decline in Arctic multiyear sea ice coverage: 1993–2009. *Geophysical Research Letters* 37. doi:10.1029/2010GL044678

Lee CC, Sheridan SC (2012) A six-step approach to developing future synoptic classifications based on GCM output. International Journal of Climatology 32:1792–1802. doi:10.1002/joc.2394

Markus T, Stroeve JC, Miller J (2009) Recent changes in Arctic sea ice melt onset, freezeup, and melt season length. Journal of Geophysical Research 114, C12024. doi:10.1029/2009JC005436

Maslanik J, Drobot S, Fowler C, Emery W, Barry R (2007) On the Arctic climate paradox and the continuing role of atmospheric circulation in affecting sea ice conditions. Geophysical Research Letters 34, L03711. doi:10.1029/2006GL028269

Moore GWK (2012) Decadal variability and a recent amplification of the summer Beaufort Sea High. Geophysical Research Letters 39, L10807. doi:10.1029/2012GL051570

Mote TL (1998) Mid-tropospheric circulation and surface melt on the Greenland ice sheet. Part II: synoptic climatology. International Journal of Climatology 18:131–145

Ogi M, Wallace JM (2012) The role of summer surface wind anomalies in summer Arctic sea ice extent in 2010 and 2011. Geophysical Research Letters 39, L09704. doi:10.1029/2012GL051330

Overland JE (2009) Meteorology of the Beaufort Sea. *Journal of Geophysical Research* 114: C00A07. doi:10.1029/2008JC004861

Overland JE, Francis JA, Hanna E, Wang M (2012) The recent shift in early summer Arctic atmospheric circulation. *Geophysical Research Letters* 39:L19804. doi:10.1029/2012GL053268

Rogers JC (1978) Meteorological factors affecting interannual variability of summertime ice extent in the Beaufort Sea. Monthly Weather Review 106:890–897

Serreze MC, Barrett AP (2011) Characteristics of the Beaufort Sea high. Journal of Climate 24:159–182

Serreze MC, Barrett AP, Stroeve JC, Kindig DN, Holland MM (2009) The emergence of surface-based Arctic amplification. Cryosphere 3:11–19

Simmonds I (2015) Comparing and contrasting the behavior of Arctic and Antarctic sea ice over the 35 year period 1979–2013. Annals of Glaciology 56:18–28. doi:10.3189/2015AoG69A909

Stroeve JC, Barrett A, Serreze M, Schweiger A (2014a) Using records from submarine, aircraft and satellite to evaluate climate model simulations of Arctic sea ice thickness. The Cryosphere Discussions 8:2179–2212. doi:10.5194/tcd-8-2179-2014

Stroeve JC, Markus T, Boisvert L, Miller J, Barrett A (2014b) Changes in Arctic melt season and implications for sea ice loss. Geophysical Research Letters 41:1216–1225. doi:10.1002/2013GL058951

Tang Q, Zhang X, Francis JA (2014) Extreme summer weather in northern mid-latitudes linked to a vanishing cryosphere. Nature Climate Change 4:45–50. doi:10.1038/NCLIMATE2065

Vihma T (2014) Effects of arctic sea ice decline on weather and climate: a review. Surveys in Geophysics 35: 1175–1214. doi:10.1007/s10712-014-9284-0

Wendler G, Moore B, Galloway K (2014) Strong temperature increase and shrinking sea ice in arctic Alaska. The Open Atmospheric Science Journal 8:7–15

Wood KR, Overland JE, Salo SA, Bond NA, Williams WJ, Dong X (2013) Is there a "new normal" climate in the Beaufort Sea? Polar Research 32:19552. doi:10.3402/polar.v32i0.19552

Wu Q, Zhang J, Zhang X, Tao W (2014) Interannual and long-term changes of atmospheric circulation over the Chukchi and Beaufort Seas. Journal of Climate 27:4871–4889

Xia W, Xie H, Changqing K (2014) Assessing trend and variation of Arctic sea-ice extent during 1979–2012 from a latitude perspective of ice edge. Polar Research 33:21249. doi:10.3402/polar.v33.21249

Yarnal B (1993) *Synoptic Climatology in Environmental Analysis: A primer*. Belhaven Press, 195 pp.